

Heating a residential building using the heat generated in the lithium ion battery pack by the electrochemical process

Saeed Alqaed^a

^a Mechanical Engineering Department, College of Engineering, Najran University, Najran 61441, Saudi Arabia



ARTICLE INFO

Keywords:
Energy saving
Building
Lithium-ion battery
Cooling

ABSTRACT

This article simulates the cooling of three packs of lithium-ion batteries using airflow in a ventilation channel. Battery packs include 12 cell batteries. Air heated by the battery is used to provide some of the energy needed for a two-story residential unit in a cold, dry environment. The energy required for this building is estimated using Design Builder software for different months of the year, and the ability to supply this energy is measured by cooling the batteries. By changing the air velocity in the range of 0.01 to 0.02 m/s and seven arrangements of battery packs in the ventilation channel, the temperature values of the battery cells, the outlet temperature of the channel, etc. are estimated. COMSOL 5.5 Multiphysics software is used to simulate the ventilation channel with battery packs. The results show that the average and optimal temperature of the battery cells can be reduced to 4.14 and 11.01 °C, respectively, by enhancing the air velocity. However, the increment in air velocity reduces the air outlet temperature, so that the maximum reduction is 4.23 °C with doubling the velocity. The designed system can supply up to 74.3% of the energy required for the house (October) from the total energy required for heating. Using this battery cooling system leads to a reduction of the amount of annual energy required by the building using urban energy sources from 17 to 14.2 kWh.

1. Introduction

Access to new energy resources is important for all countries of the world. With the limited energy resources on the one hand and the reduction of fossil fuel resources, on the other hand, finding reliable energy sources for the human future is a vital matter [1–4]. Until the necessary sources of energy are found, excessive energy consumption should be prevented [5–9]. Energy efficiency is one of the most important necessities for human life due to environmental problems of energy consumption and also limited energy resources [10–12]. Due to this important challenge, researchers have expanded their studies in the field of energy [13–17]. Some researchers in this regard have searched for new sources of available energy such as solar energy [18–22]. Other researchers, however, have explored reducing energy consumption in various devices [23–27]. They have used various methods such as the use of nanotechnology [28,29], geometry change, etc. [30–34]. Others have aimed to reduce irreversibility or optimize energy-consumed devices [35–38]. Some researchers have also studied various heat exchange devices and have tried to enhance their efficiency [39–43]. One of the most important parts of human energy consumption is the

buildings of residence, work, education, and shopping. In these places, excessive energy consumption occurs to create ventilation conditions [44–46]. By reducing energy consumption in the mentioned building, the amount of global energy consumption can be significantly reduced [47–50]. Thus, researchers have aimed to reduce energy consumption in buildings [51–53]. They used different ways such as the use of phase change materials in the building [54,55], the use of double-glazed windows [56,57], the use of double-glazed facades [58,59], the use of solar walls [60,61], and many other materials to reduce energy consumption in the building. In one of these studies, to reduce energy consumption in the building, Goya et al. [62] experimentally investigated the effect of using glass with phase change materials in a double-skin facade compared with ordinary glass and showed that the use of these glasses can significantly improve the thermal performance of the double-skin facade, especially on sunny summer days. In another article, Jaber et al. [63] utilized a part of a building's energy from the solar wall.

Batteries have a wide range of applications in electrical appliances and other devices such as solar panels [64–68]. Batteries can store electrical energy and release the required electricity. The battery heats

PII of original article: [https://doi.org/S2352-152X\(23\)02347-2](https://doi.org/S2352-152X(23)02347-2).

E-mail address: saalqaed@nu.edu.sa.

<https://doi.org/10.1016/j.est.2021.103553>

Received 5 October 2021; Received in revised form 29 October 2021; Accepted 5 November 2021

Available online 11 December 2021

2352-152X/© 2021 Elsevier Ltd. All rights reserved.

Table 1

Governing equations for battery and electrochemical process.

$\frac{\partial(\rho C_p T)}{\partial t} - \nabla \cdot (k \nabla T) = \sigma_+ \nabla \phi_+ ^2 - \sigma_- \nabla \phi_- ^2 + \dot{q}_{ECH} + \dot{q}_{short} + \dot{q}_{abuse}$	Differential equations of battery thermal and electric field
$\dot{q}_{totabl} = \dot{q}_{joule} + \dot{q}_{entropy}$	The total heat generated in the battery
$\dot{q}_{totabl} = \dot{q}_{joule} + \dot{q}_{entropy}$	Heat generated by the internal resistance of the cell
$\dot{q}_{entropy} = -IT\left(\frac{\partial V_{ocv}}{\partial T}\right) = -T\Delta S \frac{i}{nF}$	Heat generated due to entropy change due to chemical reaction
$\dot{q}_{entropy} = -IT\left(\frac{\partial V_{ocv}}{\partial T}\right) = -T\Delta S \frac{i}{nF}$	Entropy change
$\Delta G = -nFV_{ocv}$	Gibbs energy changes

up during the operation (charging and discharging). Due to technological advances and the need to charge and discharge batteries faster and reduce their operating time, the amount of heat generated in the batteries is significant [69–72]. If the battery does not cool down, especially at high charge and discharge rates, it may explode. Therefore, different researchers have done studies on batteries [73–77]. Using various cooling methods such as using nanofluids, microchannels, fins, etc., they aimed to enhance heat transfer in the heat exchangers [78–82]. Rao et al. [80] investigated a thermal management system for lithium-ion iron phosphate. Ling et al. [83] examined the thermal management system of hybrid electric vehicles with an air-cooled strategy. The thermal behavior of the battery, including the amount of heat generation and the heat transfer method, should be considered.

Energy saving in buildings has been mentioned as a necessity to reduce energy consumption. Reducing energy consumption in this area can reduce energy consumption in the world. Batteries have found wide applications. One of the most important uses of batteries is to use them to store electricity from solar panels in buildings. Batteries generate considerable heat during charging and discharging, especially at high charging and discharging rates. If you do not cool down and dissipate this heat, the battery will be seriously damaged. Due to these two important challenges mentioned in this paper, the heat generated by a battery is used to heat a building. For this purpose, the cooling of a lithium-ion battery is first simulated. Then, the heated fluid in the battery is used to heat a building. The battery is cooled and part of the heat required for a building is provided simultaneously. Briefly, the innovation of the present work is the cooling of a battery pack with special geometry and the use of its generated heat as a part of the energy required for a house.

2. Problem definition

The lithium-ion battery is one of the rechargeable batteries in which lithium ions move from the negative electrode toward the positive one during discharging mode and move from positive to negative electrodes during the charging process. A battery is a device that converts chemical

energy directly into electrical energy. A battery consists of one or more voltaic cells, which generate electricity due to the chemical reactions of oxides and reductions. Each voltage cell consists of two electrodes that are filled with an electrolyte. Conchannel solution electrolyte

Table 2

Material of materials used in the building [84].

Density (Kg/m ³)	Thermal conductivity (W/mK)	Specific heat (J/kgK)	Material
1700	0.25	1000	Asphalt felt
1900	1	840	Brick
2110	1.15	1000	Asphalt
2000	1.15	920	Mortar
2300	1.75	1000	Concrete
1300	0.34	840	Concrete with pumice
1000	0.3	1000	Air layer
1000	1.15	840	Plaster and soil
2500	2.9	840	Granite
1300	0.7	1000	Plaster
3000	1.4	1000	Mosaic
2300	1.3	840	Ceramic

Table 3

Placement order of different layers and their thickness [84].

Thickness (m)	Layers	Building components
0.1	Concrete with pumice	Floor connected to the ground
0.02	Mortar	
0.03	Mosaic	
0.005	Plaster	
0.02	Plaster and soil	Floor between stories
0	Air layer	
0.1	Concrete	
0.08	Concrete with pumice	
0.02	Mortar	
0.1	Ceramic	
0.04	Asphalt	The roof of the building
0.03	Asphalt felt	
0.02	Mortar	
0.05	Concrete with pumice	
0.1	Concrete	
0.4	Air layer	
0.02	Plaster and soil	
0.005	Plaster	
0.02	Granite	Outer wall
0.02	Mortar	
0.2	Brick	
0.02	Plaster and soil	
0.005	Plaster	
0.005	Plaster	Outer wall
0.02	Plaster and soil	
0.1	Brick	
0.02	Plaster and soil	
0.005	Plaster	

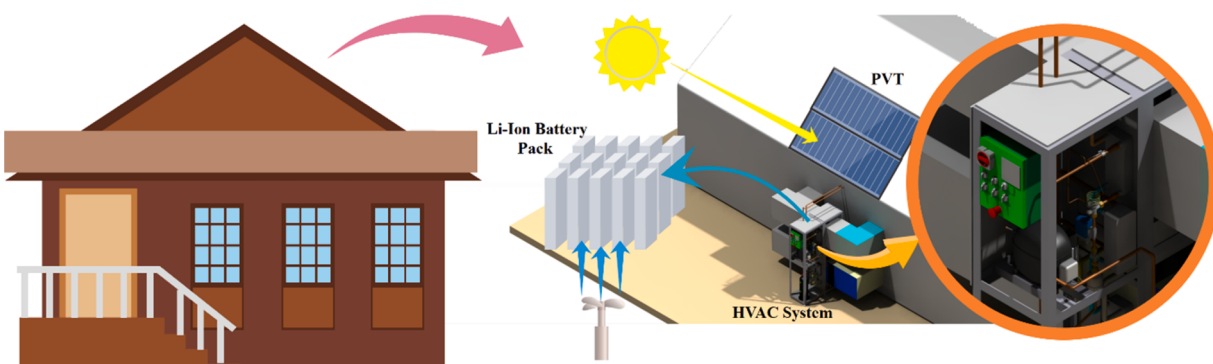


Fig. 1. Schematic of a complete air channel with battery packs.

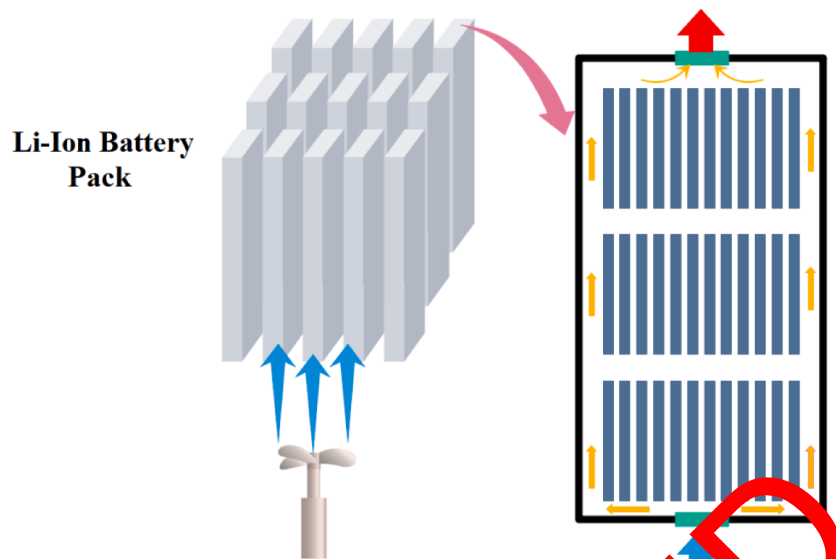


Fig. 2. Schematic of the lithium-ion battery pack with boundary conditions (air inlet and outlet and the placement of batteries).

Table 4

Outlet temperature values at two different velocities different numbers of elements for Model 2.

v (m/s)	736,000	845,000	921,000	1,020,000	1,113,000
0.01	292.98	292.65	292.48	292.40	292.39
0.02	288.53	287.96	287.72	287.62	287.61

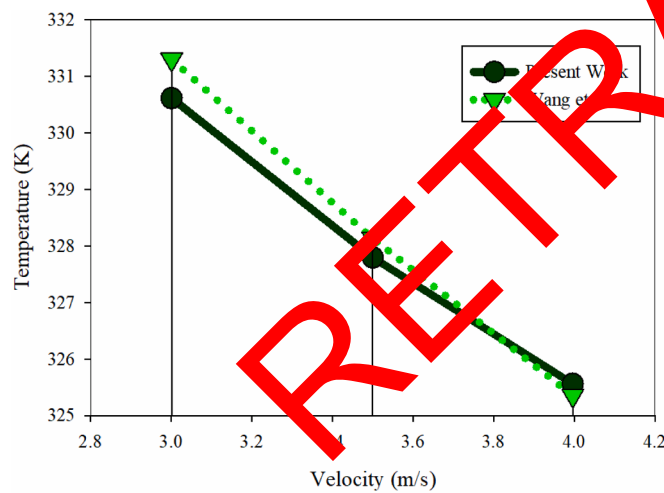


Fig. 3. Maximum temperature generated on the battery versus air velocity at the battery pack inlet: comparison between the results of the present study and the ones of Wang et al. [86].

contains ions. Electroactive compounds are usually dissolved in the electrolyte, which can react chemically with the electrodes and convert the chemical energy into electrical energy by transferring charge at the electrode-electrolyte interface. The output voltage of a battery is directly related to the chemical nature of the cell's electrochemical reaction. During the electrochemical process that takes place in the battery, heat is generated in the battery, which leads to a decrease in battery performance (Table 1 presents the equations governing the battery thermal field) that should be removed.

To cool the battery cells, they are placed in an air channel. The system consists of three battery packs with 12 cells on a plate in each

pack. Air enters the ventilation channel with constant velocity and exits it after cooling the battery cells and then heat the residential unit. The dimensions of the channel and its schematic figure can be seen in Fig. 1.

The building under study includes a 6-m-high building located in a city with a cold and dry climate. The area of each floor is 135 m² and its height is 2.8 m. There are five and four 2 × 2-m² windows in the north and south facades of the building, respectively, which are double-glazed and filled with argon gas. The total heat transfer coefficient is 2.5 W/m²·K. The indoor design temperature is 27.1 °C for summer and 23.5 °C for winter. Tables 2 and 3 show the properties and order of placement of materials in the walls. It is assumed that the battery is working during the day and night (charging or discharging modes) to provide energy. According to the location of barrettes in each system, the cooling system size is 40 × 50 × 30 cm.

3. Governing equations

The equations govern the ventilation system; including lithium-ion batteries are presented. The flow inside the air channel is laminar and steady and the airflow is assumed to be Newtonian and incompressible. Radiation heat transfer, gravity, and viscosity loss are neglected.

Mass conservation equation:

$$\frac{\partial \rho}{\partial t} + \nabla \cdot (\rho \vec{V}) = 0 \quad (1)$$

By applying the assumption of constant density and steady-state, this equation becomes the following.

$$\nabla \cdot (\vec{V}) = 0 \quad (2)$$

Momentum conservation equation:

The momentum conservation equation is Newton's second law and its vector differential expression is as follows:

$$\frac{\partial(\rho \vec{v})}{\partial t} + \nabla \cdot (\rho \vec{v} \vec{v}) = \nu p + \nabla \cdot (\bar{\tau}) + \rho \vec{g} \quad (3)$$

$$\bar{\tau} = \mu \left[(\nabla \vec{V} + \nabla \vec{V}^T) - \frac{2}{3} \nabla \cdot \vec{V} I \right]$$

By applying the Boussinesq approximation and considering that the problem is steady, this equation is simplified to the following form.

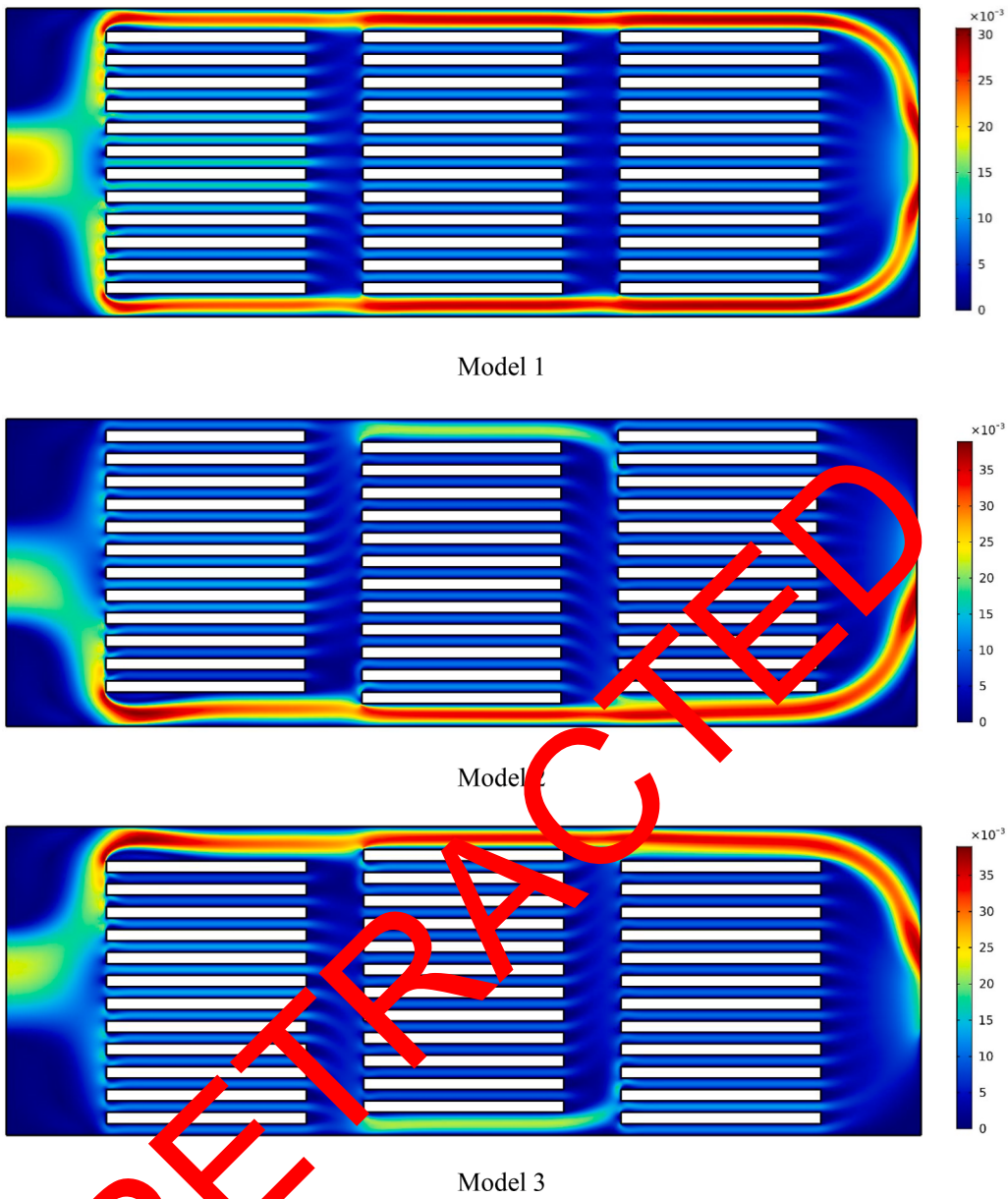


Fig. 4. Velocity contours for different models of 3 battery packs with 12 battery cells in each pack at a velocity of 0.015 m/s.

$$\frac{\partial(\vec{V})}{\partial t} + \nabla \cdot (\vec{V} \vec{V}) = -\frac{\nabla p}{\rho} + \nabla \cdot (\vec{v}) - \frac{(T - T_0)}{T_0} g \\ \vec{v} = \mu / \rho (\nabla \vec{V} + \nabla \vec{V}^T) \quad (4)$$

Energy conservation equation:

This equation is the first law of thermodynamics, which becomes a differential equation for temperature assuming that the specific heat capacity of air is constant. These assumptions are steady and incompressible flow:

$$\rho \nabla \cdot (\vec{V} T) = \nabla \cdot (k_{eff} \nabla T) \quad (5)$$

4. Numerical method, boundary conditions, and validation

In this paper, DesignBuilder software is used to model the sample space. This software uses the EnergyPlus-based solver to analyze the heat transfer processes governing the building. Accordingly,

DesignBuilder performs heat transfer and airflow calculations using the thermal balance method and air zonal method. COMSOL 5.5 Multi-physics software is also used to simulate the ventilation channel. For this purpose, the equations governing the airflow in the ventilation channel are algebraized by using the finite element method. Further details of the solution can be found in the reference [85].

As shown in Fig. 2, air enters the ventilation channel at a constant velocity and temperature of 283.15 K and exits at a constant pressure equal to atmospheric pressure.

Table 4 presents the outlet temperature values of the cooling system for two different velocities. It can be seen that no changes in the output temperature occur when the number of elements exceeds 102,000 elements. Hence, this number of elements is selected for the simulations. It is noteworthy that the number of elements in this table is rounded.

The results of Wang et al. [86] are used to validate the present paper. They examined the battery thermal management system using the air-cooled system. They examined several placement configurations and also provided results by proposing models for inlet and outlet

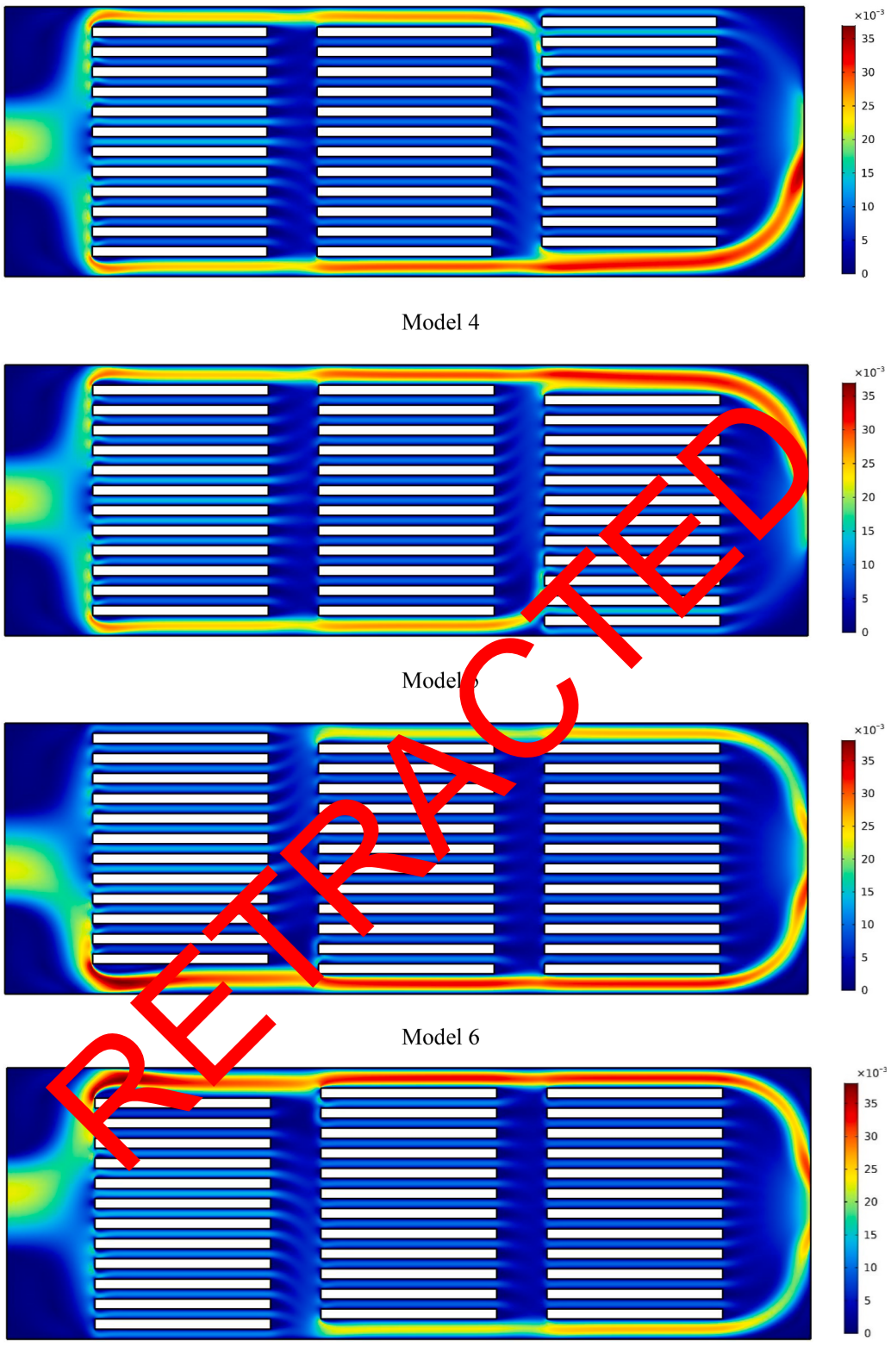


Fig. 4. (continued).

arrangements. They proposed the Z-Type model for battery heat management and showed that this model improves battery performance compared to other models and also reduces the maximum battery temperature from 3.42 to 6.4 K. In this study, the results obtained from their studies with the results obtained from the model used in this study have

been used. According to the Fig. 3, it can be seen that the maximum temperature decreases with the air velocity. Thus, the comparison is performed for maximum temperature. According to the diagram, it can be seen that the use of this model provides acceptable results with a maximum error of 1.93%. Therefore, it will be used as a criterion for

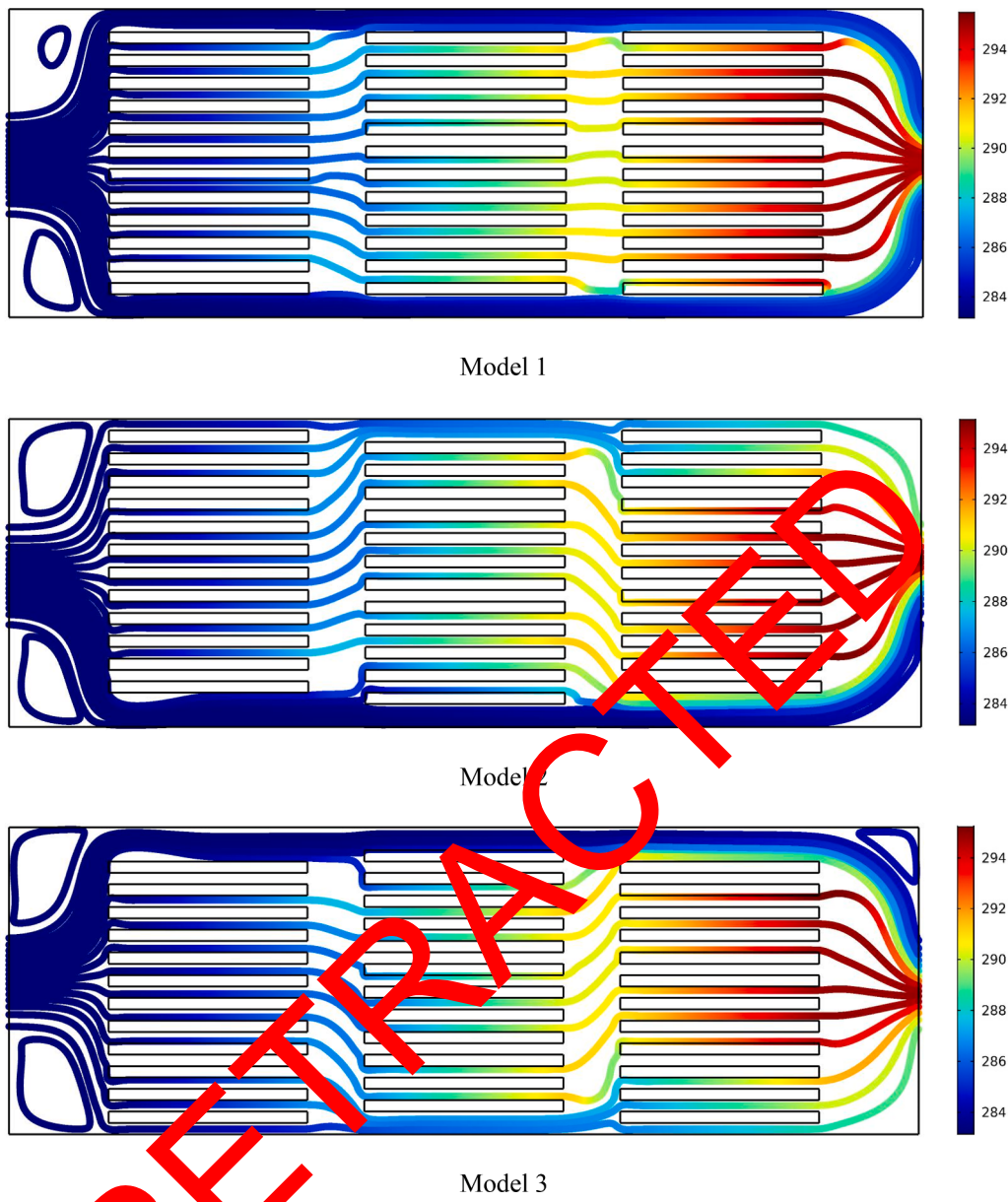


Fig. 5. Airflow path lines for different models of 3 battery packs with 12 battery cells in each pack at a velocity of 0.015 m/s.

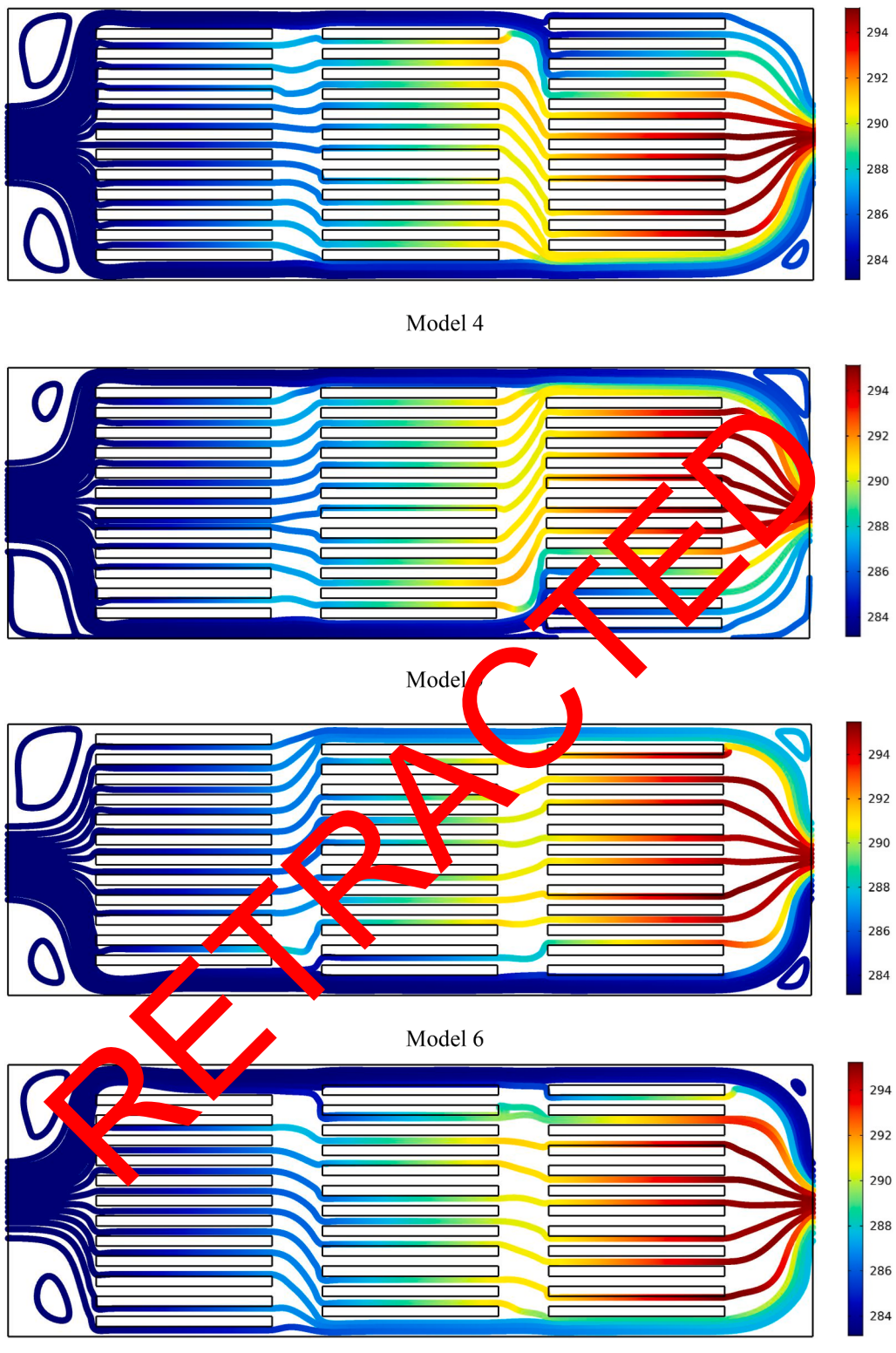
performing calculations.

5. Results and discussion

Fig. 4 demonstrates velocity contours for different models of 3 battery packs with 12 battery cells in each pack at a velocity of 0.015 m/s. The air tends to go in a direction with a lower pressure drop. Therefore, the amount of air velocity is higher in parts that there is no battery cell. By changing the location of the battery pack, more air passes through these areas. The lowest maximum velocity is seen in model 1. In this model, due to the placement of the battery pack in the middle of the channel, there is a large space for air to pass on either side of the channel. Hence, the amount of air velocity is also increased less. In other models, due to the absence of battery cells, the maximum velocity is close to each other. In models 2 and 3, which have two primary and last battery packs on one side and a middle battery pack on the other side, the maximum velocity is also higher. The first and the last pack of batteries have a greater impact on the maximum velocity than the

original pack as well as the direction where the highest air velocity occurs. The velocity values among the battery cells in the first pack of the battery are higher than the other two packs.

Fig. 5. shows airflow path lines for different models of 3 battery packs with 12 battery cells in each pack at a velocity of 0.015 m/s. Model 1 has streamlines with a temperature symmetrical to the horizontal midline of the ventilation channel. This model has a symmetrical flow due to its geometric symmetry. In other models, the amount of flow passing through one side of the ventilation channel is always higher, leading to that the amount of fluid temperature in this area is lower. The passage of more fluid in this area means faster airflow, which reduces the time for heat exchange in this area and therefore the temperature is lower. The maximum air temperature always occurs in the middle of the ventilation channel. The temperature is higher in this area due to the passage of air between the battery cells and heat transfer with the battery cells. This area has a lower velocity due to more pressure drop and has more time to exchange heat with the battery cells. There are two high vortices in the entrance corners of the air channel and two small

**Fig. 5. (continued).**

vortices in the corners of the air channel at the exit. The air stationary in these areas causes these vortices.

Fig. 6. depicts isothermal lines for different models of 3 battery packs with 12 battery cells in each pack at a velocity of 0.01 and 0.02 m/s. In the first model, it can be seen that the isotherms are symmetric for both velocities. But, in other models of battery packs, one side of the channel

is warmer than the other side. More airflow from one side of the channel compared to the other sides causes this issue. The batteries in the middle of the battery pack are at a higher temperature than the side batteries. The air velocity at the sides of the channel is higher, which makes the batteries have lower temperatures in those areas. Also, the first pack of batteries is at a lower temperature than the other two packs. The outlet-

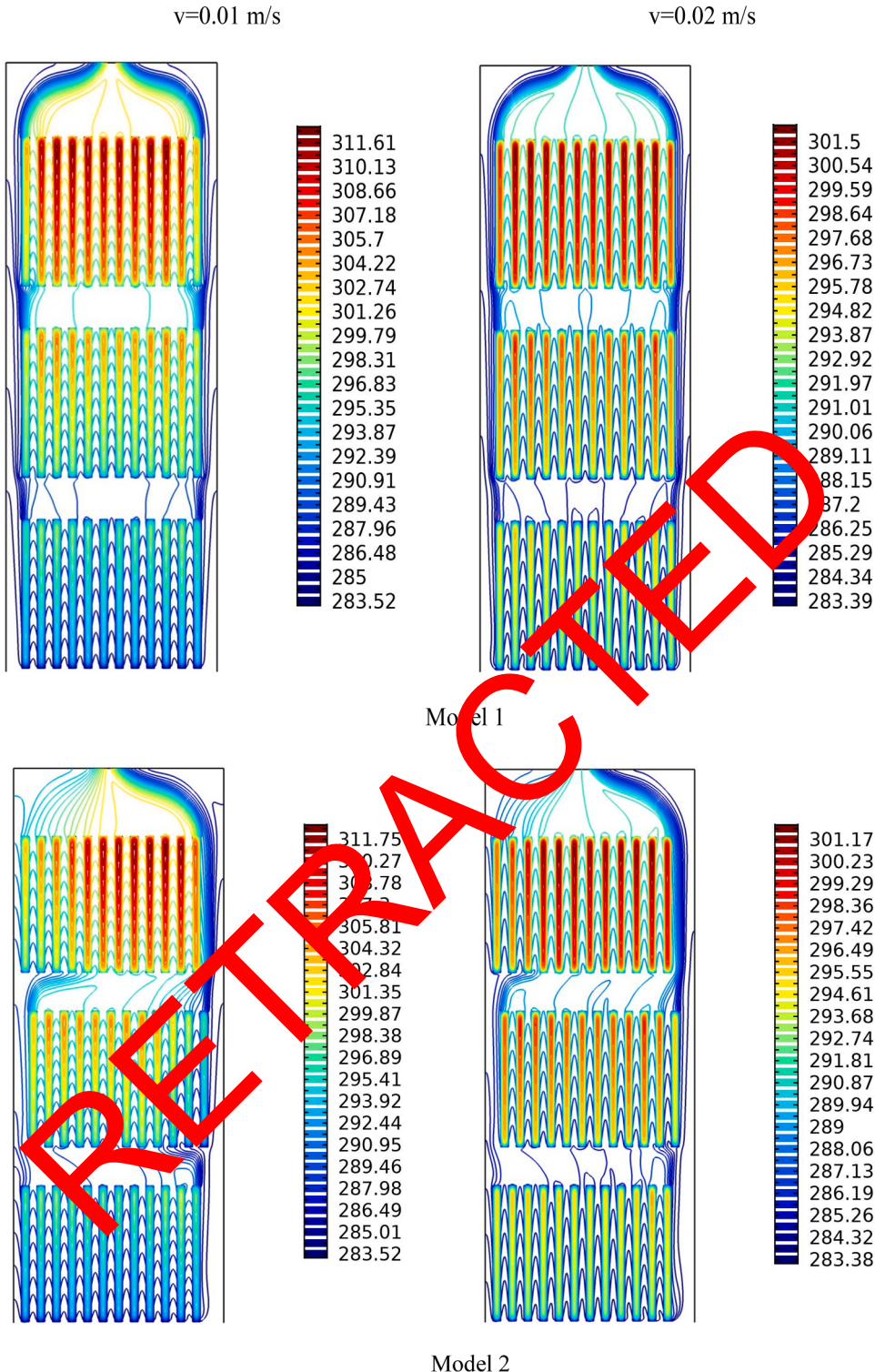


Fig. 6. Isothermal lines for different models of 3 battery packs with 12 battery cells in each pack at a velocity of 0.01 and 0.02 m/s.

side packs have the hottest batteries. The batteries laced in the first pack have a lower temperature than the other two packs due to contact with air. The last pack is warmer due to contact with air at higher temperatures (air is at the temperature of previous batteries). The increase in air velocity in the channel causes the temperature of the batteries in the battery packs to decrease. Air velocity causes the air to be in the channel in less time and as a result, its temperature in each section of the channel

is less than the low-velocity case. Thus, it can exchange heat efficiently with the battery cells and cool the batteries. Besides, the increase in air velocity causes the battery cells in a battery pack to have a closer temperature to each other and the temperature of the middle batteries to be closer to the side batteries.

Fig. 7. illustrates the average temperature of 36 battery cells for three different velocities and different models of three battery packs.

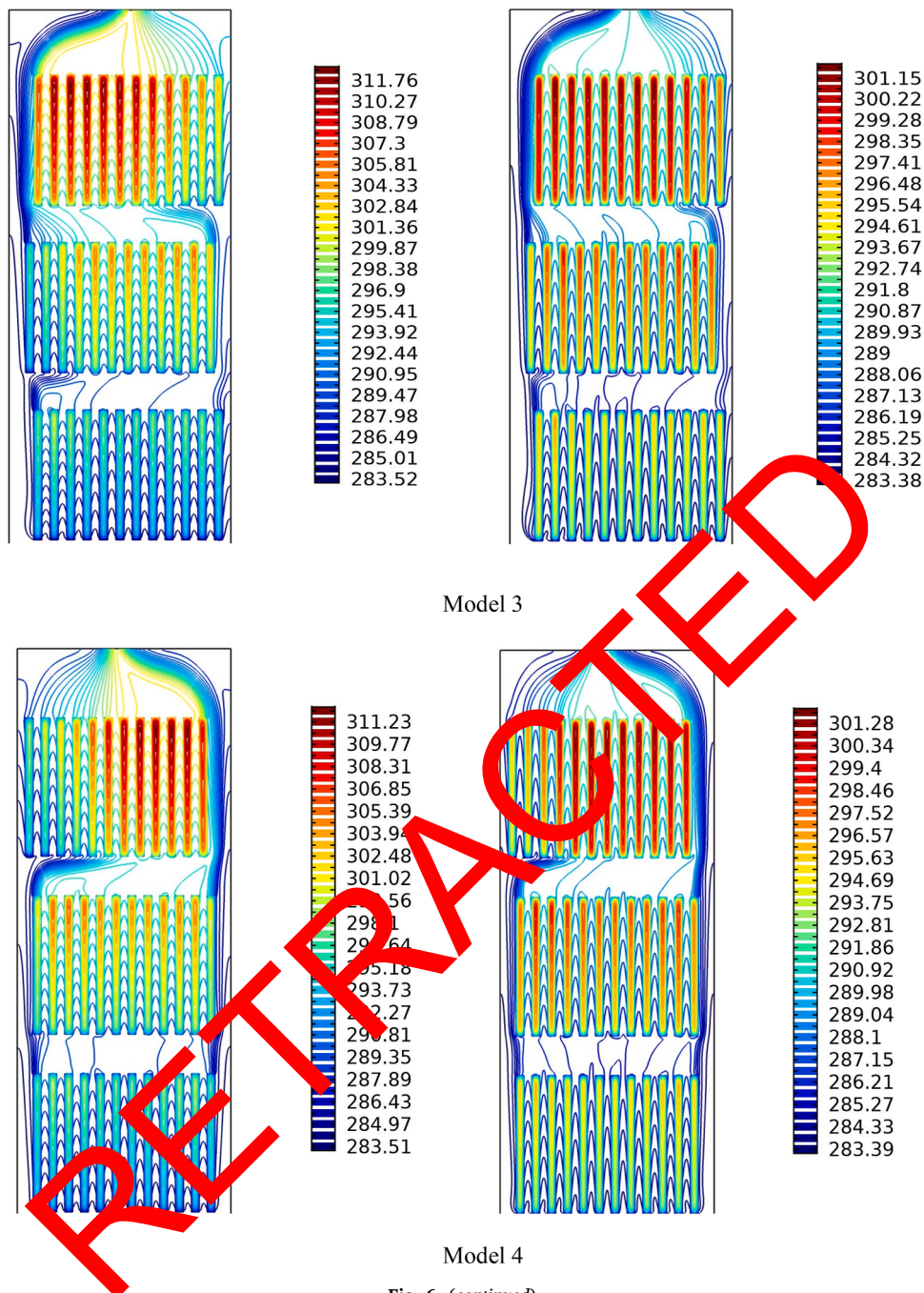


Fig. 6. (continued).

Specifically, an increment in the air velocity causes the amount of average temperature of the batteries inside the channel to decrease. A reduction in battery temperature occurs for all battery pack modes by enhancing the fluid velocity. An enhancement in the air velocity from 0.01 to 0.015 m/s reduces the average temperature. Due to the similarity of the arrangements of packs, the average temperatures of models 2, 3, 4, 5, 6, and 7 are very close to each other. The minimum average temperatures of battery cells correspond to models 4 and 5, and the maximum one is related to model 1. This is valid for all velocities. It can be seen that an increment in the velocity from 0.01 to 0.02 m/s reduces the temperature of models 4 and 5 by 4 °C, while reducing the temperature of model 1 by 5.14 °C, indicating that an enhancement in the air velocity has a greater impact on model 1.

Fig. 8. depicts the maximum temperature on 36 battery cells for three different velocities and different models of three battery packs. The

maximum battery cell temperature occurs on the middle batteries of the pack at the outlet side of the channel for all cases. These batteries are at a higher temperature than other battery cells due to the passage of airflow with a lower velocity and higher temperature. An enhancement in the air velocity causes the maximum temperature to be lower than the average temperature of the battery cells. Increasing the air velocity allows the air to receive more heat from the battery cells and cool them. The highest maximum battery cell temperatures for velocities of 0.01, 0.015, and 0.02 m/s correspond to models 2, 3, and 1, respectively. The minimum temperature of the battery cell for velocities of 0.01, 0.015, and 0.02 m/s corresponds to models 4, 5, and 3, respectively. The maximum and minimum temperature reduction occurs for model 3 and models 4 and 5, respectively. These values are 11.01 and 10.33 °C.

Fig. 9. shows the maximum temperature for 36 battery cells and three different velocities and different models of three battery packs. An

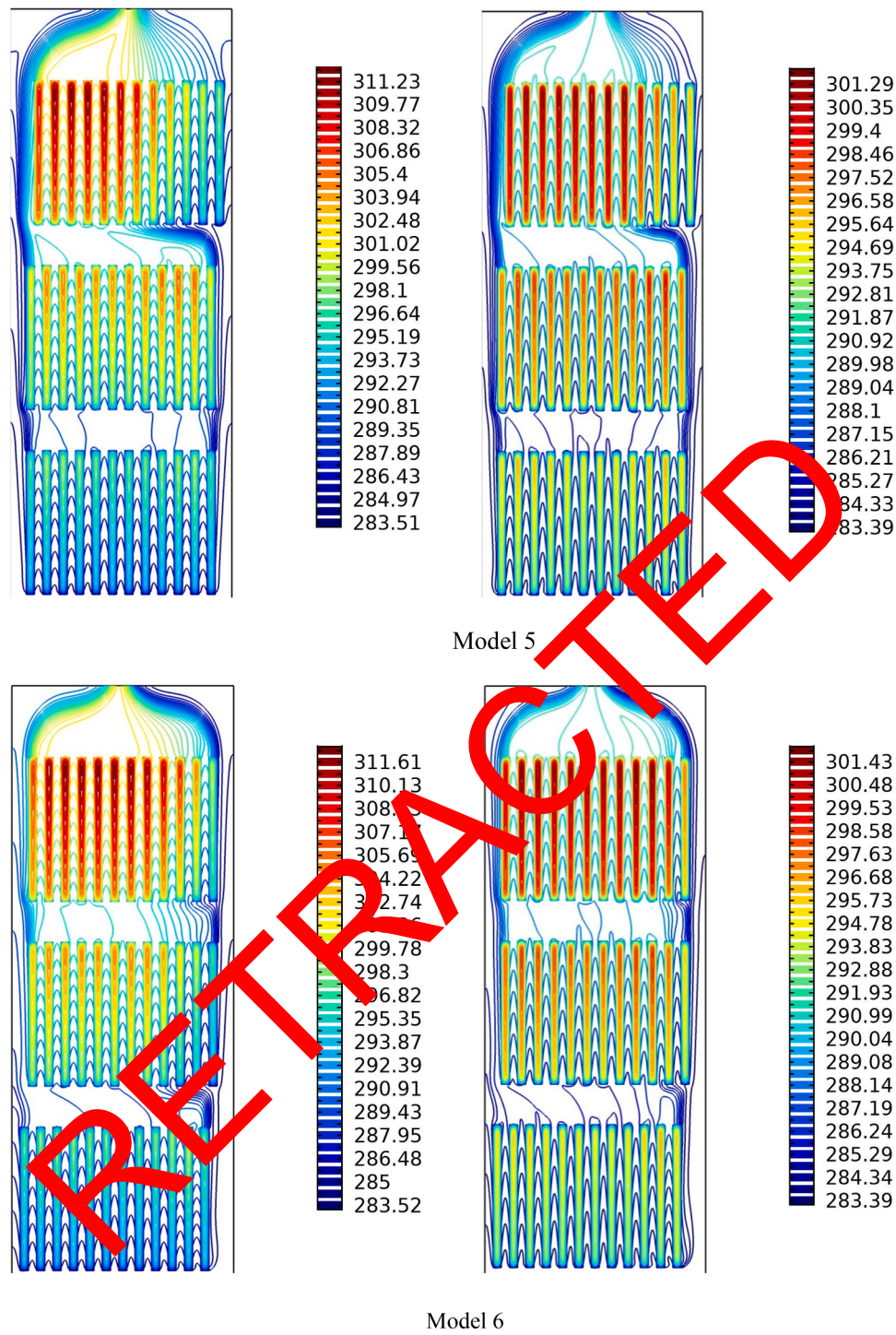


Fig. 6. (continued).

increment in the air velocity reduces the heat exchange time between the battery and the air in the air channel. Hence, the air remains less next to the battery cells and the cells have less temperature. As a result, the increase in velocity causes the amount of air temperature in the ventilation channel to decrease. The output temperature difference between various models of battery packs at low air velocities is greater than that at high velocities. The maximum air outlet temperature at different velocities corresponds to models 2 and 3, while the minimum outlet air temperature is related to model 1. Enhancing the air velocity from 0.01 to 0.02 m/s causes a slight decrease in the inlet and outlet temperature of the air for models 1, 2, 4, and 6, respectively, which is 4.23, 4.98, 4.6,

and 4.45 °C. The maximum and minimum temperature reduction corresponds to models 2 and 1, respectively. Therefore, with the doubling of the air velocity in the ventilation channel, the difference between the inlet and outlet air temperature is reduced by less than 50%. Considering the constant heat capacity of the air, more heat can be transferred from the battery packs to the air at higher air velocities.

Fig. 10. demonstrates the heat transfer coefficient on 36 battery cells for three different velocities and different models of three battery packs. Increasing the air velocity slightly enhances the heat transfer coefficient on the battery cells. An increment in the air velocity makes the velocity boundary layer thinner on the battery cell. Therefore, due to the

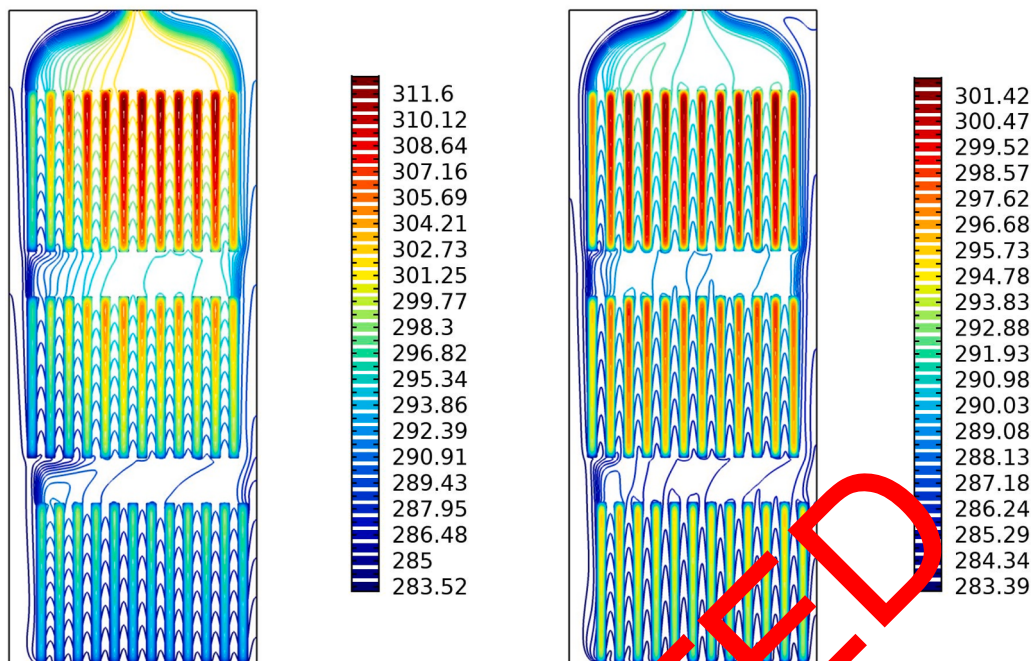


Fig. 6. (continued).
Model 7

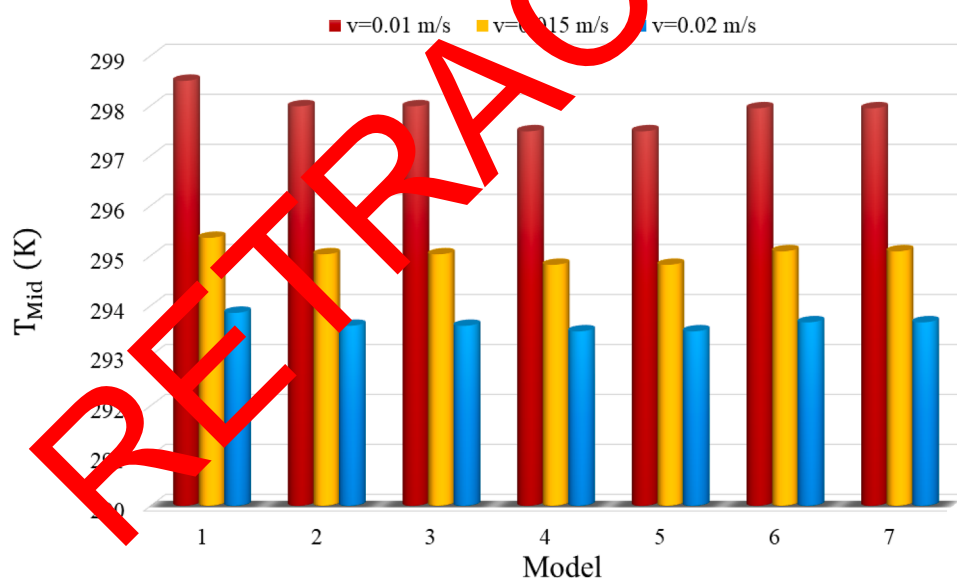


Fig. 7. The average temperature of 36 battery cells for three different velocities and different models of three battery packs.

constant Prandtl number, the thickness of the thermal boundary layer decreases, which causes the temperature gradient near the outer layer of the battery cells to enhance, resulting in a slightly higher heat transfer coefficient. Also, an enhancement in the air velocity intensifies the amount of temperature difference between the battery and the fluid, especially in the last pack of the battery, leading to an increase in the amount of heat transfer coefficient. Model 1 has the minimum heat transfer coefficient at all velocities. However, this model has the maximum heat transfer coefficient by enhancing the velocity; its value increases by 105% by doubling the velocity. The maximum heat transfer coefficient is different for different velocities. Models 2 and 3 have a maximum heat transfer coefficient for the velocity of 0.01 m/s. Model 2 has a maximum heat transfer coefficient for the velocity of 0.015 m/s

and models 4 and 5 have a maximum heat transfer coefficient for the velocity of 0.02 m/s. The lowest heat transfer coefficient corresponds to models 2 and 3 by doubling the velocity, which is by 102%.

Fig. 11. illustrates the pressure drop in the ventilation channel for three different velocities and different models of three battery packs. Increasing the air velocity between the battery cells enhances the amount of pressure drop. An increment in the air velocity causes the velocity difference in the close layer of the stationary battery cells to increase. The vertical velocity gradient enhances the amount of shear stress on the battery cells. An increment in the shear stresses generally causes an intensification in the pressure drop in the ventilation channel. The amount of pressure drop is the same for different models, and only model 1 has a greater pressure drop than other ones.

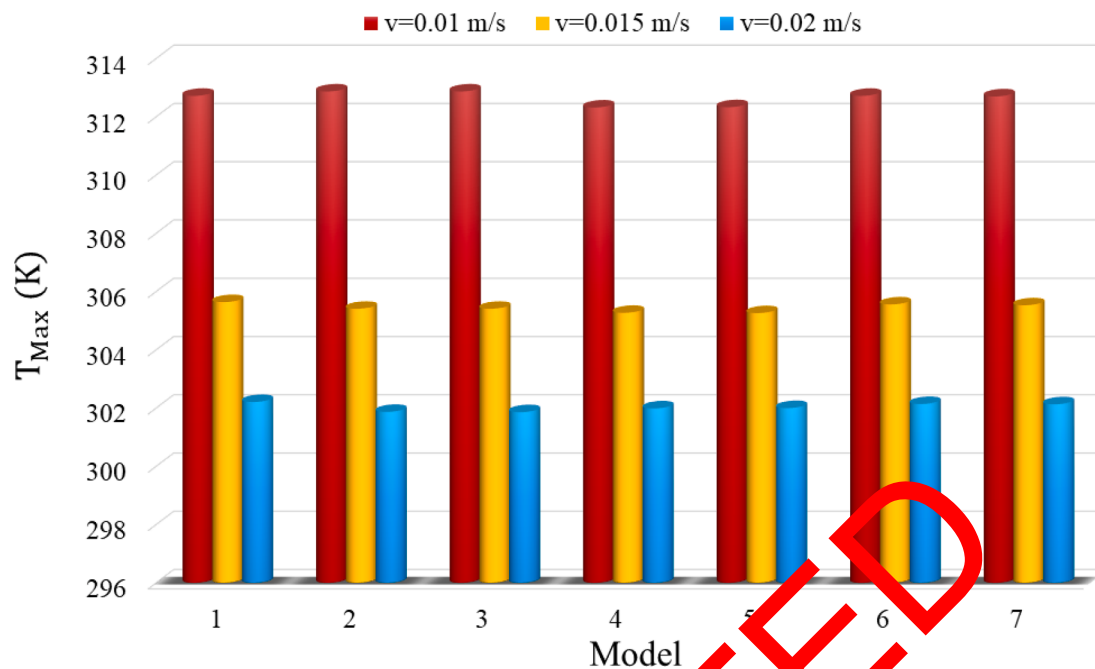


Fig. 8. Maximum temperature on 36 battery cells for three different velocities and different models of three battery packs.

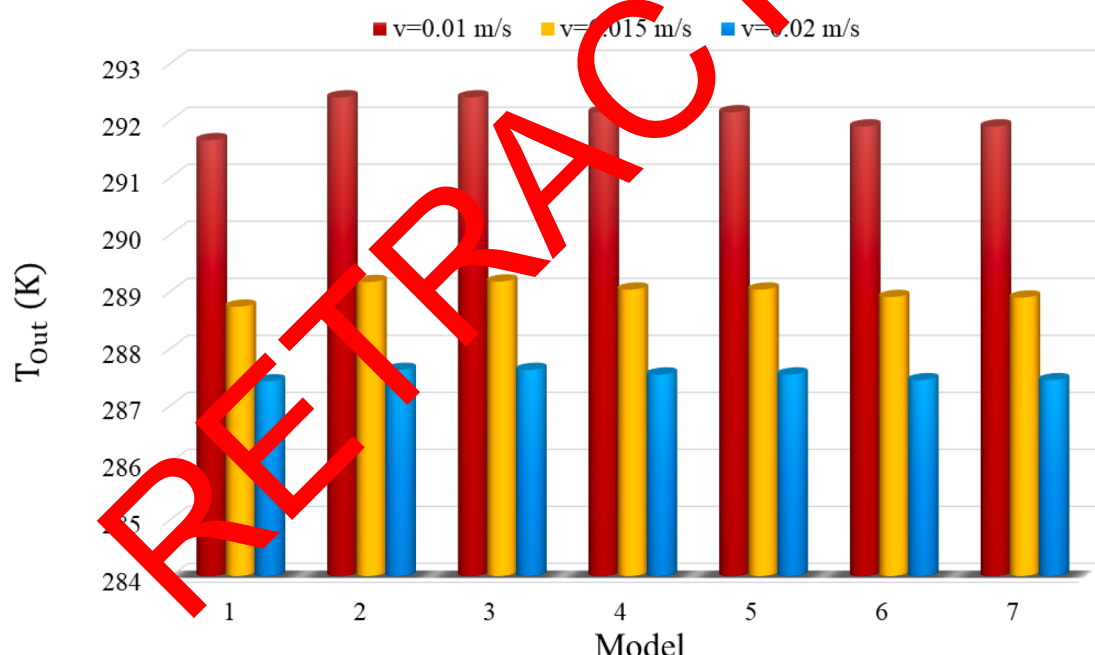


Fig. 9. Maximum temperature for 36 battery cells and three different velocities and different models of three battery packs.

Fig. 12. depicts the percentage of supply energy from the total energy required by the building for different months of the year at different air velocities in the ventilation channel. It is seen that the higher the air velocity in the channel, despite the battery packs, causes to receive a greater amount of energy required from the battery packs. In the cold seasons, the percentage of supply energy by cooling the batteries from the total energy is reduced due to the higher need of the building for heating energy. The supplied energy from batteries is constant in different months and the percentage of supply energy from batteries decreases with the increase of building energy needs. In January and

February, the contribution of supply energy from the total energy is minimum and this contribution is maximum in June and October. Also, in summer, the figure does not show a number due to the lack of need for heating energy.

Fig. 13. illustrates the annual heating energy required by the building at different air velocities in the ventilation channel. It can be seen that the annual energy required by the building is usually about 17 kWh. Now, in the presence of the battery packs, the amount of energy required for the home heating system from fossil fuels is reduced by using the ventilation system. This amount of energy can also be reduced by about 14.2 kWh. In the presence of the battery, using air with higher velocity in the ventilation channel causes the amount of energy produced by this

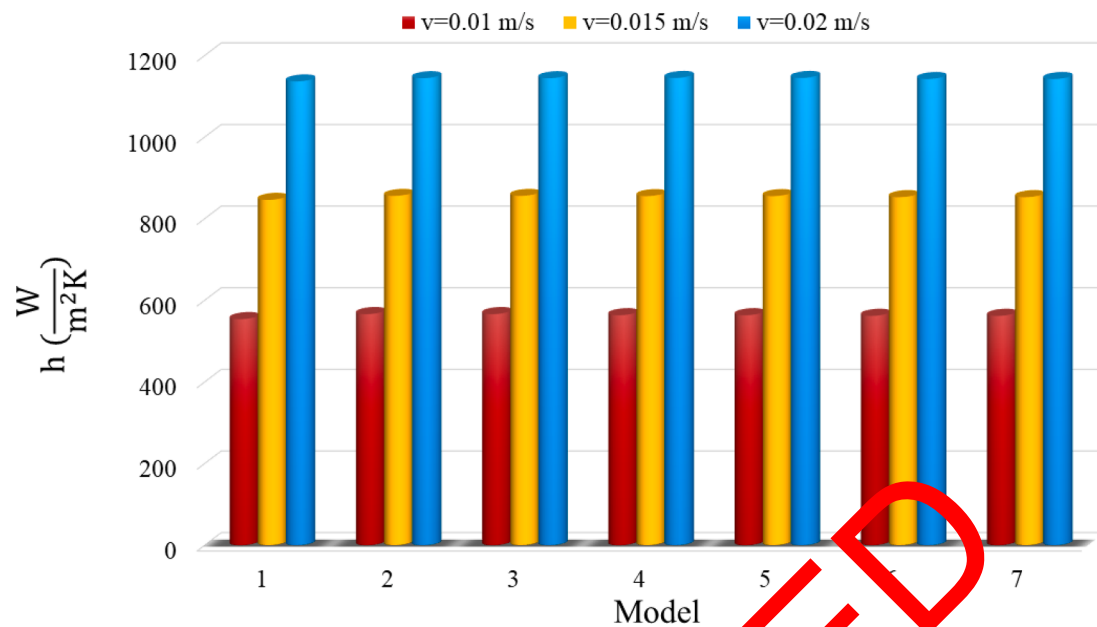


Fig. 10. Heat transfer coefficient on 36 battery cells for three different velocities and different models of three battery packs.

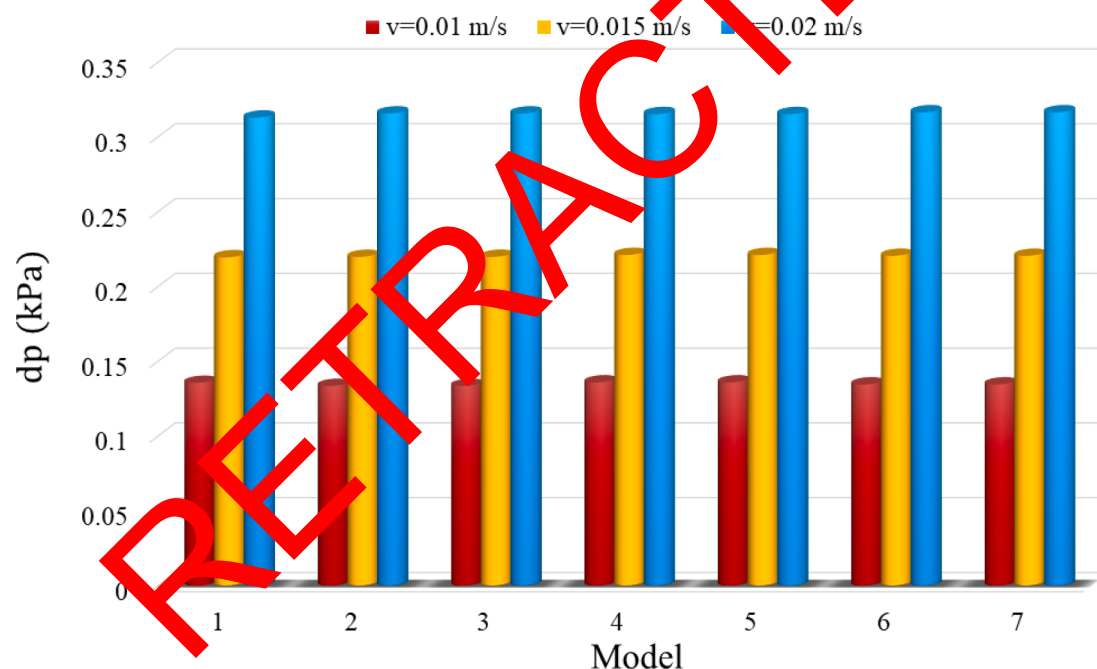


Fig. 11. The pressure drop in the ventilation channel for three different velocities and different models of three battery packs.

system to increase due to a higher heat transfer rate from the battery to the air. As a result, the energy required by the building is reduced.

Conclusions

This paper simulates the airflow around three lithium-ion battery packs with 12 battery cells in each battery pack in a ventilation channel to heat the building. The air velocity is changed between 0.01 and 0.02 m/s for different models of battery packs, and the values of battery cell temperature, air outlet temperature, heat transfer coefficient, etc. are determined. The results of this study demonstrate:

1. An increment in the air velocity in the ventilation channel causes the average and maximum temperature values of the battery cells and the air outlet temperature from the channel to decrease.
2. Enhancing the air velocity intensifies the values of heat transfer coefficient on the battery cells and the pressure drop in the ventilation channel.
3. The minimum average temperature of battery cells corresponds to models 4 and 5 and the maximum average temperature is related to model 1. Doubling the air velocity for these models reduces the average temperature of the battery cells by 4 and 5.14 °C.
4. Doubling the air velocity can reduce the maximum temperature of the battery cells to 11.01 °C.

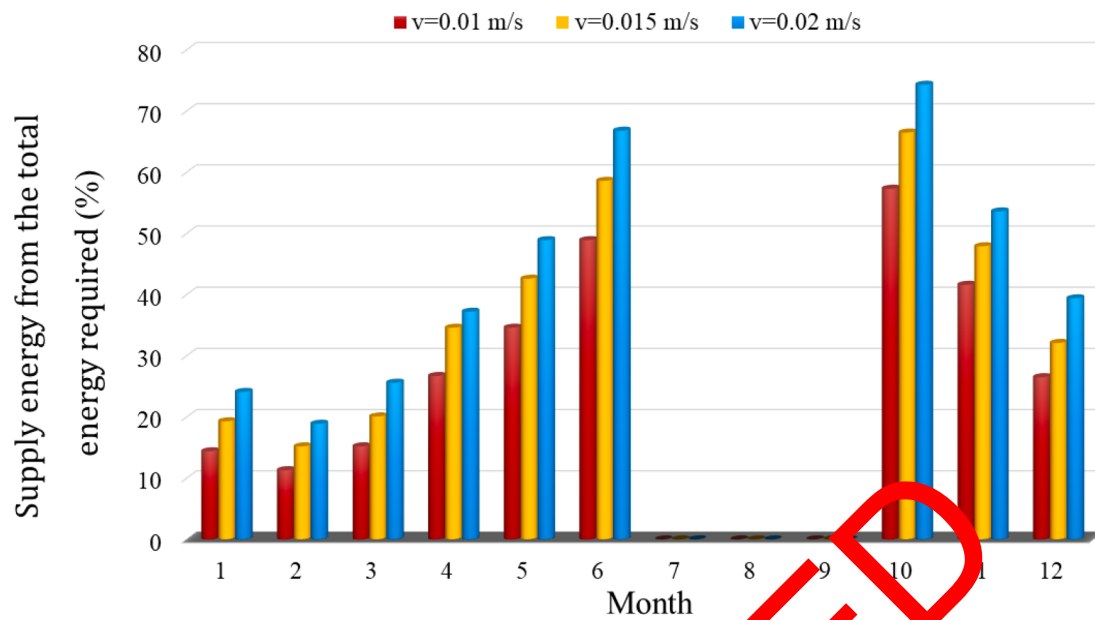


Fig. 12. Percentage of supply energy from the total energy required by the building for different months of the year at different air velocities in the ventilation channel.

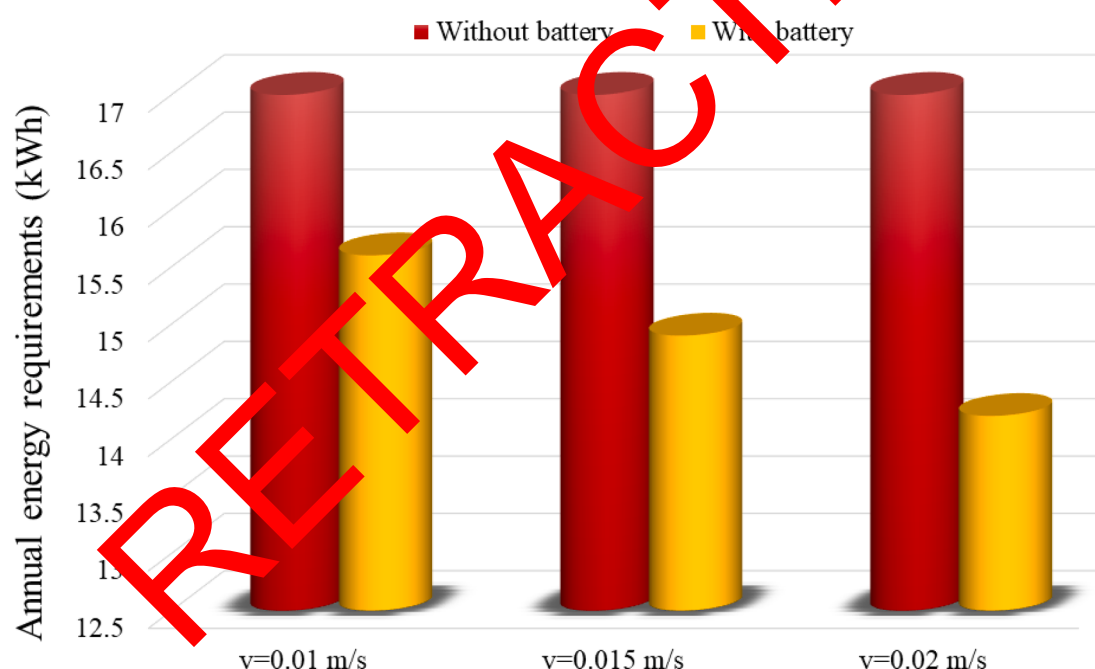


Fig. 13. Annual heating energy required by the building at different air velocities in the ventilation channel.

5. The lowest decrease in outlet temperature by increasing velocity from 0.01 to 0.02 m/s corresponds to model 1, which has a value equal to 4.23 °C.
6. The minimum value of heat transfer coefficient occurs for model 1. However, doubling the inlet velocity gives the maximum heat transfer coefficient (105%) for this model.
7. By placing three battery packs in the ventilation channel when air velocity is 0.02 m/s, 74.3% of the supply energy required by the building can be provided in the best condition in October.
8. For air velocities of 0.01, 0.015, and 0.02 m/s, the values of 1.4, 2.1, and 2.8 kWh of the annual supply energy required for the building can be obtained from the cooling of the battery packs.

Declaration of Competing Interest

The authors declare that they have no known competing financial interests or personal relationships that could have appeared to influence the work reported in this paper.

Funding and Acknowledgement

The authors would like to express their Gratitude's to the ministry of education and the deanship of scientific research – Najran University – Kingdom of Saudi Arabia for their financial and Technical support under code number (code NU-/SERC/10/648). We are also thankful to the Department of Mechanical Engineering, College of Engineering, Najran

University, Najran.

References

- [1] C.H.H. Wong, M. Cai, C. Ren, Y. Huang, C. Liao, S. Yin, Modelling building energy use at urban scale: a review on their account for the urban environment, *Build. Environ.* 205 (2021), 108235, <https://doi.org/10.1016/j.buildenv.2021.108235>.
- [2] S.-C. Zhang, X.-Y. Yang, W. Xu, Y.-J. Fu, Contribution of nearly-zero energy buildings standards enforcement to achieve carbon neutral in urban area by 2060, *Adv. Clim. Change Res.* (2021), <https://doi.org/10.1016/j.accre.2021.07.004>.
- [3] J. Mustafa, S. Alqaed, R. Kalbasi, Challenging of using CuO nanoparticles in a flat plate solar collector- Energy saving in a solar-assisted hot process stream, *J. Taiwan Inst. Chem. Eng.* 124 (2021) 258–265.
- [4] S. Alqaed, J. Mustafa, F. Almehmadi, Design and Energy Requirements of a Photovoltaic-Thermal Powered Water Desalination Plant for the Middle East, *Int. J. Environ. Res. Public Health* 18 (3) (2021), 1001.
- [5] A. Hajatzadeh Pordanjani, S. Aghakhani, M. Afrand, B. Mahmoudi, O. Mahian, S. Wongwises, An updated review on application of nanofluids in heat exchangers for saving energy, *Energy Convers. Manage.* 198 (2019), 111886, <https://doi.org/10.1016/j.enconman.2019.111886>.
- [6] M.R. Akhtari, I. Shayegh, N. Karimi, Techno-economic assessment and optimization of a hybrid renewable earth - air heat exchanger coupled with electric boiler, hydrogen, wind and PV configurations, *Renew. Energy* 148 (2020) 839–851, <https://doi.org/10.1016/j.renene.2019.10.169>.
- [7] M. Torabi, N. Karimi, M. Torabi, G.P. Peterson, C.J. Simonson, Generation of entropy in micro thermofluidic and thermochemical energy systems-A critical review, *Int. J. Heat Mass Transf.* 163 (2020), 120471, <https://doi.org/10.1016/j.ijheatmasstransfer.2020.120471>.
- [8] A. Amiramad, A. Maglad, J. Mustafa, G. Cheraghian, Loading PCM Into Buildings Envelope to Decrease Heat Gain-Performing Transient Thermal Analysis on Nanofluid Filled Solar System, *Front. Energy Res.* 9 (2021), 727011.
- [9] S. Alqaed, J. Mustafa, K.P. Hallinan, R. Elhashmi, Hybrid CHP/Geothermal Borehole System for Multi-Family Building in Heating Dominated Climates, *Sustainability* 12 (18) (2020), 7772.
- [10] A.H. Pordanjani, S. Aghakhani, M. Afrand, M. Sharifpur, J.P. Meyer, H. Xu, H. M. Ali, N. Karimi, G. Cheraghian, Nanofluids: physical phenomena, applications in thermal systems and the environment effects: a critical review, *J. Clean. Prochanell.* (2021), 128573, <https://doi.org/10.1016/j.jclepro.2021.128573>.
- [11] A. Khalil, M.A. Alharthi, S. Alqaed, E.M.A. Mokheimer, R. Kumar, Analysis and Assessment of Tower Solar Collector Driven Trigeneration System, *J. Sol. Energy Eng.* 142 (5) (2020), 051003.
- [12] J. Mustafa, S. Alqaed, M. Sharifpur, Incorporating nano-scale material in solar system to reduce domestic hot water energy demand, *Sustain. Energy Technol. Assess.* 49 (2022), 101735.
- [13] X. Peng, Z. Liu, D. Jiang, A review of multiphase energy conversion in wind power generation, *Renew. Sustain. Energy Rev.* 147 (2021), 111172, <https://doi.org/10.1016/j.rser.2021.111172>.
- [14] Q.u. Zaman, Z. Wang, S. Zaman, S.F. Rasool, Investigating the nexus between education expenditure, female employers, renewable energy consumption and CO2 emission: evidence from China, *J. Clean. Prochanell.* 312 (2021), 127823, <https://doi.org/10.1016/j.jclepro.2021.127823>.
- [15] M. Yang, E.-Z. Wang, Y. Hou, The relationship between manufacturing growth and CO2 emissions: does renewable energy consumption matter? *Energy* 232 (2021), 121032, <https://doi.org/10.1016/j.energy.2021.121032>.
- [16] C. Estebe, Y. Liu, M. Vahab, M. Sussman, A. Moradikazerouni, K. Shoele, A low mach number, adaptive mesh method for simulating multi-phase flows in cryogenic fuel tanks.
- [17] A. Moradikazerouni, M. Vahab, K. Shoele, A 0D/1D nodal-CFD method of cylindrical pressurized tank, in: *Advances in Fluid Dynamics Meeting Abstracts*, 2020 p. T01_014.
- [18] X. Li, D. Gui, Z. Zhao, X. Li, X. Gu, Y. Hua, H. Zhong, Operation optimization of electrical-heating integrated energy system based on concentrating solar power plant hybridized with combined heat and power plant, *J. Clean. Prod.* 289 (2021), 125712, <https://doi.org/10.1016/j.jclepro.2020.125712>.
- [19] D. Wang, L. Hu, H. Du, Y. Liu, J. Huang, Y. Xu, J. Liu, Classification, experimental assessment, modeling methods and evaluation metrics of Trombe walls, *Renew. Sustain. Energy Rev.* 124 (2020), 109772, <https://doi.org/10.1016/j.rser.2020.109772>.
- [20] J.A. Duffie, W.A. Beckman, N. Blair, *Solar Engineering of Thermal Processes, Photovoltaics and Wind*, John Wiley & Sons, 2020.
- [21] M. Edalatpour, J.P. Solano, Thermal-hydraulic characteristics and exergy performance in tube-on-sheet flat plate solar collectors: effects of nanofluids and mixed convection, *Int. J. Therm. Sci.* 118 (2017) 397–409, <https://doi.org/10.1016/j.ijthermalsci.2017.05.004>.
- [22] R.A. Agathokleous, S.A. Kalogirou, Double skin facades (DSF) and building integrated photovoltaics (BIPV): a review of configurations and heat transfer characteristics, *Renew. Energy* 89 (2016) 743–756, <https://doi.org/10.1016/j.renene.2015.12.043>.
- [23] M.-W. Tian, S. Rostami, S. Aghakhani, A.S. Goldanlou, C. Qi, A techno-economic investigation of 2D and 3D configurations of fins and their effects on heat sink efficiency of MHD hybrid nanofluid with slip and non-slip flow, *Int. J. Mech. Sci.* 189 (2021), 105975, <https://doi.org/10.1016/j.ijmecsci.2020.105975>.
- [24] L. Jiang, Y. Wang, X. Wang, F. Ning, S. Wen, Y. Zhou, F. Zhou, Electrohydrodynamic printing of a dielectric elastomer actuator and its application in tunable lenses. *Composites. Part A, Appl. Sci. Manuf.* 147 (2021), 106461, <https://doi.org/10.1016/j.compositesa.2021.106461>.
- [25] M. Afrand, S. Farahat, A.H. Nezhad, G. Ali Sheikhzadeh, F. Sarhaddi, 3-D numerical investigation of natural convection in a tilted cylindrical annulus containing molten potassium and controlling it using various magnetic fields, *Int. J. Appl. Electromagnet. Mech.* 46 (2014) 809–821, <https://doi.org/10.3233/JAE-141975>.
- [26] M. Afrand, S. Farahat, A.H. Nezhad, G.A. Sheikhzadeh, F. Sarhaddi, Numerical simulation of electrically conchanneling fluid flow and free convective heat transfer in an annulus on applying a magnetic field, *Heat Trans. Res.* 45 (8) (2014) 749–766, <https://doi.org/10.1615/HeatTransRes.2014007285>.
- [27] A. Moradikazerouni, K. Shoele, Computational study of Rayleigh-Bernard convection in a cylindrical pressurized cryogenic tank, *Bull. Am. Phys. Soc.* (2021).
- [28] R. Alizadeh, J.M.N. Abad, A. Ameri, M.R. Mohebbi, A. Mehdizadeh, D. Zhao, N. Karimi, A machine learning approach to the prediction of transport and thermodynamic processes in multiphysics systems - heat transfer in a hybrid nanofluid flow in porous media, *J. Taiwan Inst. Chem. Eng.* 124 (2021) 290–306, <https://doi.org/10.1016/j.jtice.2021.03.043>.
- [29] L. Govone, M. Torabi, L. Wang, N. Karimi, Effects of nanofluid and radiative heat transfer on the double-diffusive forced convection in microreactors, *J. Therm. Anal. Calorim.* 135 (1) (2019) 45–59, <https://doi.org/10.1007/s10973-018-7027-z>.
- [30] S. Aghakhani, A.H. Pordanjani, A. Karimipour, A. Abdollahi, M. Afrand, Numerical investigation of heat transfer in a power-law non-Newtonian fluid in a C-Shaped cavity with magnetic field effect using finite difference lattice Boltzmann method, *Comput. Fluids* 176 (2018) 61–67.
- [31] A.H. Pordanjani, S. Aghakhani, Numerical investigation of natural convection and irreversibilities between two inclined concentric cylinders in presence of uniform magnetic field and radiation, *Heat Trans. Eng.* (2021) 1–21, <https://doi.org/10.1080/01457630.2021.199973>.
- [32] X. Chen, T. Wang, Y. Wang, Z. Cao, A fault diagnosis method considering meteorological factors for transmission networks based on P systems, *Entropy* 23 (8) (2021), <https://doi.org/10.3390/e23081008>.
- [33] Wang, T., Li, W., Zhao, J., Guo, X., Terzija, V. (2020). A rough set-based bio-inspired fault diagnosis method for electrical substations. *International journal of electrical power & energy systems*, 119, 105961. <https://doi.org/10.1016/j.ijepes.2020.105961>.
- [34] T. Wang, Y. Wei, J. Wang, T. Huang, H. Peng, X. Song, M.J. Pérez-Jiménez, A weighted corrective fuzzy reasoning spiking neural P system for fault diagnosis in power systems with variable topologies, *Eng. Appl. Artif. Intell.* 92 (2020), 262–270, <https://doi.org/10.1016/j.engappai.2020.103680>.
- [35] Y. Zheng, S. Yaghoubi, A. Dezfulizadeh, S. Aghakhani, A. Karimipour, I. Tlili, Free convection/radiation and entropy generation analyses for nanofluid of inclined square enclosure with uniform magnetic field, *J. Therm. Anal. Calorim.* 141 (1) (2020) 635–648, <https://doi.org/10.1007/s10973-020-09497-y>.
- [36] Z. Huang, T. Wang, W. Liu, L. Valencia-Cabrera, M.J. Pérez-Jiménez, P. Li, Z. W. Geem, A fault analysis method for three-phase induction motors based on spiking neural P systems, *Complexity* (New York, N.Y.) 2021 (2021) 1–19, <https://doi.org/10.1155/2021/2087027>.
- [37] R. Kalbasi, M. Afrand, J. Alsarraf, M.-D. Tran, Studies on optimum fins number in PCM-based heat sinks, *Energy* 171 (2019) 1088–1099, <https://doi.org/10.1016/j.energy.2019.01.070>.
- [38] H. Park, A design of air flow configuration for cooling lithium ion battery in hybrid electric vehicles, *J. Power Sources* 239 (2013) 30–36, <https://doi.org/10.1016/j.jpowsour.2013.03.102>.
- [39] M. Bahrami, M. Akbari, S.A. Bagherzadeh, A. Karimipour, M. Afrand, M. Goodarzi, Develop 24 dissimilar ANNs by suitable architectures & training algorithms via sensitivity analysis to better statistical presentation: measure MSEs between targets & ANN for Fe–Cu/O₂-Water nanofluid, *Physica A* 519 (2019) 159–168, <https://doi.org/10.1016/j.physa.2018.12.031>.
- [40] S.-R. Yan, S. Aghakhani, A. Karimipour, Influence of a membrane on nanofluid heat transfer and irreversibilities inside a cavity with two constant-temperature semicircular sources on the lower wall: applicable to solar collectors, *Phys. Scr.* 95 (8) (2020), 085702, <https://doi.org/10.1088/1402-4896/ab93e4>.
- [41] R. Habib, N. Karimi, B. Yadollahi, M.H. Doranegard, L.K.B. Li, A pore-scale assessment of the dynamic response of forced convection in porous media to inlet flow modulations, *Int. J. Heat Mass Transf.* 153 (2020), 119657, <https://doi.org/10.1016/j.ijheatmasstransfer.2020.119657>.
- [42] R. Habib, B. Yadollahi, N. Karimi, M.H. Doranegard, On the unsteady forced convection in porous media subject to inlet flow disturbances-A pore-scale analysis, *Int. Commun. Heat Mass Transf.* 116 (2020), 104639, <https://doi.org/10.1016/j.icheatmasstransfer.2020.104639>.
- [43] A. Saeed, N. Karimi, G. Hunt, M. Torabi, On the influences of surface heat release and thermal radiation upon transport in catalytic porous microreactors—A novel porous-solid interface model, *Chem. Eng. Process. - Process Intensif.* 143 (2019), 107602, <https://doi.org/10.1016/j.cep.2019.107602>.
- [44] N. Soares, N. Rosa, J.J. Costa, A.G. Lopes, T. Matias, P.N. Simões, L. Durães, Validation of different numerical models with benchmark experiments for modelling microencapsulated-PCM-based applications for buildings, *Int. J. Therm. Sci.* 159 (2021), 106565, <https://doi.org/10.1016/j.ijthermalsci.2020.106565>.
- [45] P. Wang, Z. Liu, L. Zhang, Sustainability of compact cities: a review of inter-building effect on building energy and solar energy use, *Sustain. Cities Soc.* 72 (2021), 103035, <https://doi.org/10.1016/j.scs.2021.103035>.
- [46] G. Tian, Y. Fan, M. Gao, H. Wang, H. Zheng, J. Liu, C. Liu, Indoor thermal environment of thin membrane structure Buildings: a review, *Energy Build.* 234 (2021), 110704, <https://doi.org/10.1016/j.enbuild.2020.110704>.

- [47] L. Gibbons, S. Javed, A review of HVAC solution-sets and energy performance of nearly zero-energy multi-story apartment buildings in Nordic climates by statistical analysis of environmental performance certificates and literature review, *Energy* 238 (2022), 121709, <https://doi.org/10.1016/j.energy.2021.121709>.
- [48] Y. Dutil, D. Rousse, S. Lassue, L. Zalewski, A. Joulin, J. Virgone, F. Kuznik, K. Johannes, J.-P. Dumas, J.-P. Bédécarrats, A. Castell, L.F. Cabeza, Modeling phase change materials behavior in building applications: comments on material characterization and model validation, *Renew. Energy* 61 (2014) 132–135, <https://doi.org/10.1016/j.renene.2012.10.027>.
- [49] S. Barbosa, K. Ip, Perspectives of double skin façades for naturally ventilated buildings: a review, *Renew. Sustain. Energy Rev.* 40 (2014) 1019–1029, <https://doi.org/10.1016/j.rser.2014.07.192>.
- [50] N. Soares, J.J. Costa, A.R. Gaspar, P. Santos, Review of passive PCM latent heat thermal energy storage systems towards buildings' energy efficiency, *Energy Build.* 59 (2013) 82–103, <https://doi.org/10.1016/j.enbuild.2012.12.042>.
- [51] O. Saadatian, K. Sopian, C.H. Lim, N. Asim, M.Y. Sulaiman, Trombe walls: a review of opportunities and challenges in research and development, *Renew. Sustain. Energy Rev.* 16 (8) (2012) 6340–6351, <https://doi.org/10.1016/j.rser.2012.06.032>.
- [52] D. Heim, Isothermal storage of solar energy in building construction, *Renew. Energy* 35 (4) (2010) 788–796, <https://doi.org/10.1016/j.renene.2009.09.005>.
- [53] H.-Y. Chan, S.B. Riffat, J. Zhu, Review of passive solar heating and cooling technologies, *Renew. Sustain. Energy Rev.* 14 (2) (2010) 781–789, <https://doi.org/10.1016/j.rser.2009.10.030>.
- [54] B. Pandey, R. Banerjee, A. Sharma, Coupled EnergyPlus and CFD analysis of PCM for thermal management of buildings, *Energy Build.* 231 (2021), 110598, <https://doi.org/10.1016/j.enbuild.2020.110598>.
- [55] H. Akeiber, P. Nejat, M.Z.A. Majid, M.A. Wahid, F. Jomehzadeh, I. Zeynali Famileh, J.K. Calatut, B.R. Hughes, S.A. Zaki, A review on phase change material (PCM) for sustainable passive cooling in building envelopes, *Renew. Sustain. Energy Rev.* 60 (2016) 1470–1497, <https://doi.org/10.1016/j.rser.2016.03.036>.
- [56] M.A. Shameri, M.A. Alghoul, K. Sopian, M.F.M. Zain, O. Elayeb, Perspectives of double skin façade systems in buildings and energy saving, *Renew. Sustain. Energy Rev.* 15 (3) (2011) 1468–1475, <https://doi.org/10.1016/j.rser.2010.10.016>.
- [57] J. Zhou, Y. Chen, A review on applying ventilated double-skin facade to buildings in hot-summer and cold-winter zone in China, *Renew. Sustain. Energy Rev.* 14 (4) (2010) 1321–1328, <https://doi.org/10.1016/j.rser.2009.11.01>.
- [58] Y. Tao, H. Zhang, L. Zhang, G. Zhang, J. Tu, L. Shi, Ventilation performance of a naturally ventilated double-skin façade in buildings, *Renew. Energy* 167 (2021) 184–198, <https://doi.org/10.1016/j.renene.2020.11.073>.
- [59] A. Jankovic, F. Goia, Impact of double skin facade constructional features on heat transfer and fluid dynamic behaviour, *Build. Environ.* 196 (2021), 107796, <https://doi.org/10.1016/j.buildenv.2021.107796>.
- [60] K. Sergei, C. Shen, Y. Jiang, A review of the current work potential of a trombe wall, *Renew. Sustain. Energy Rev.* 130 (2020), 109947, <https://doi.org/10.1016/j.rser.2020.109947>.
- [61] N. Zhu, S. Li, P. Hu, F. Lei, R. Deng, Numerical investigation on performance of phase change material Trombe wall in building, *Energy* 167 (2020), 718057, <https://doi.org/10.1016/j.energy.2019.116057>.
- [62] F. Goia, M. Perino, V. Serra, Improving thermal comfort conditions by means of PCM glazing systems, *Energy Build.* 60 (2013) 447–452, <https://doi.org/10.1016/j.enbuild.2013.01.029>.
- [63] S. Jaber, S. Ajib, Optimum design of Trombe wall system in mediterranean region, *Sol. Energy* 85 (9) (2011) 1891–1898, <https://doi.org/10.1016/j.solener.2011.04.025>.
- [64] L. Yang, Q. Dai, L. Liu, D. Shao, K. Luo, C. Lam, X. Wang, Rapid sintering method for highly conductive Li₇La₃Zr₂O₁₂ ceramic electrolyte, *Ceram. Int.* 46 (8) (2020) 10917–10924, <https://doi.org/10.1016/j.ceramint.2020.01.106>.
- [65] Y. Chen, M. Sang, W. Jiang, L. Wang, J. Zou, C. Guo, Z. Ma, Fracture predictions based on a coupled chemico-mechanical model with strain gradient plasticity theory for film electrodes of Li-ion batteries, *Eng. Pract. Mech.* 253 (2021), 107866, <https://doi.org/10.1016/j.enganbmec.2021.107866>.
- [66] X. Zhang, Y. Tang, F. Zhang, C. Lv, A Novel aluminum-graphite dual-ion battery, *Adv. Energy Mater.* 6 (11) (2016), 1602588, <https://doi.org/10.1002/aenm.201502588>.
- [67] B. Ji, F. Zhang, X. Song, Y. Tang, A Novel Potassium-Ion-Based Dual-Ion Battery, *Adv. Mater. (Weinheim)* 29 (19) (2017), 1700519, <https://doi.org/10.1002/adma.201700519>.
- [68] Z. Zhang, R. Xun, L. Wang, Z. Meng, Construction of pseudocapacitive Li_xsub.2-xLa_xZnTi_xsub.3O_xsub.8 anode for fast and super-stable lithium storage, *Ceram. Int.* 47 (1) (2021) 662, <https://doi.org/10.1016/j.ceramint.2020.08.174>.
- [69] Q. Wang, B. Jiang, B. Li, Y. Yan, A critical review of thermal management models and solutions of lithium-ion batteries for the development of pure electric vehicles, *Renew. Sustain. Energy Rev.* 64 (2016) 106–128, <https://doi.org/10.1016/j.rser.2016.05.033>.
- [70] L. Lu, X. Han, J. Li, J. Hua, M. Ouyang, A review on the key issues for lithium-ion battery management in electric vehicles, *J. Power Sources* 226 (2013) 272–288, <https://doi.org/10.1016/j.jpowsour.2012.10.060>.
- [71] A. Barré, B. Deguilhem, S. Grolleau, M. Gérard, F. Suard, D. Riu, A review on lithium-ion battery ageing mechanisms and estimations for automotive applications, *J. Power Sources* 241 (2013) 680–689, <https://doi.org/10.1016/j.jpowsour.2013.05.040>.
- [72] Q. Wang, P. Ping, X. Zhao, G. Chu, J. Sun, C. Chen, Thermal runaway caused fire and explosion of lithium ion battery, *J. Power Sources* 208 (2012) 210–224, <https://doi.org/10.1016/j.jpowsour.2012.02.038>.
- [73] X. Tong, F. Zhang, B. Ji, M. Sheng, Y. Tang, Carbon-coated porous aluminum foil anode for high-rate, long-term cycling stability, and high energy density dual-ion batteries, *Adv. Mater. (Weinheim)* 28 (45) (2016) 9979–9985, <https://doi.org/10.1002/adma.201603735>.
- [74] M. Wang, C. Jiang, S. Zhang, X. Song, Y. Tang, H. Cheng, Reversible calcium alloying enables a practical room-temperature rechargeable calcium-ion battery with a high discharge voltage, *ACS Appl. Mater. Interfaces* 10 (6) (2018) 667–672, <https://doi.org/10.1038/s41557-017-00454>.
- [75] L. Li, Y. Shan, F. Zhang, X. Chen, Y. Zhang, D. Zhou, W. Cui, Improving fast and safe transfer of lithium ions in solid-state lithium batteries by porosity and channel structure of polymeric electrolyte, *ACS Appl. Mater. Interfaces* (2021), <https://doi.org/10.1021/acsmi.1c0489>.
- [76] S. Mu, Q. Jin, P. Kidkhum, X. Zhou, W. Wang, Y. Tang, Molecular grafting towards high fraction active nanodots implanted in N-doped carbon for sodium dual-ion batteries, *Natl. Sci. Rev.* 8 (7) (2020), <https://doi.org/10.1093/nsr/nwaa178>.
- [77] Y. Sun, Y. Yang, X. Shi, G. Suo, H. Chen, X. Hou, Z. Chen, Self-standing film assembly using Sm₂Sn/multiwalled carbon nanotubes encapsulated carbon fibers: a potential large-scale production material for ultra-stable sodium-ion battery anodes, *ACS Appl. Mater. Interfaces* 13 (24) (2021) 28359–28368, <https://doi.org/10.1021/acsmi.1c07152>.
- [78] H. Teng, A.P. Kjeljo, Yeow, design of direct and indirect liquid cooling systems for high- capacity, high-power lithium-ion battery packs, *SAE Int. J. Alt. Power.* 1 (2) (2012) 525–536, <https://doi.org/10.4271/2012-01-2017>.
- [79] R. Mahamud, C. Park, Reciprocating air flow for Li-ion battery thermal management to improve temperature uniformity, *J. Power Sources* 196 (13) (2011) 5685–5696, <https://doi.org/10.1016/j.jpowsour.2011.02.076>.
- [80] Z. Rao, S. Wang, G. Zhang, Simulation and experiment of thermal energy management with phase change material for ageing LiFePO₄ power battery, *Energy Convers. Manage.* 52 (12) (2011) 3408–3414, <https://doi.org/10.1016/j.enconman.2011.07.009>.
- [81] X. Duan, G.F. Naterer, Heat transfer in phase change materials for thermal management of electric vehicle battery modules, *Int. J. Heat Mass Transf.* 53 (23) (2010) 5176–5182, <https://doi.org/10.1016/j.ijheatmasstransfer.2010.07.044>.
- [82] A. Saeed, N. Karimi, M.C. Paul, Analysis of the unsteady thermal response of a Li-ion battery pack to dynamic loads, *Energy* 231 (2021), 120947, <https://doi.org/10.1016/j.energy.2021.120947>.
- [83] Z. Ling, F. Wang, X. Fang, X. Gao, Z. Zhang, A hybrid thermal management system for lithium ion batteries combining phase change materials with forced-air cooling, *Appl. Energy* 148 (2015) 403–409, <https://doi.org/10.1016/j.apenergy.2015.03.080>.
- [84] A. Handbook, HVAC Systems and Equipment, 39, chapter, 1996.
- [85] W.B. Zimmerman, Multiphysics Modeling With Finite Element Methods, World Scientific Publishing Company, 2006.
- [86] M. Wang, S. Teng, H. Xi, Y. Li, Cooling performance optimization of air-cooled battery thermal management system, *Appl. Therm. Eng.* (2021), 117242.